Pramana – J. Phys. (2025) 99:2
https://doi.org/10.1007/s12043-024-02860-w

Influence of symmetry energy on electromagnetic field during heavy-ion collisions

DHANPAT SHARMA and SUNEEL KUMAR*

Department of Physics and Astrophysics, Central University of Haryana, Mahendergarh 123 031, India
*Corresponding author. E-mail: suneelkumar@cuh.ac.in

MS received 5 February 2024; revised 23 June 2024; accepted 8 October 2024

Abstract. Heavy-ion collision simulations in intermediate energy regime using isospin quantum molecular dynamics model have been proposed as a novel means to glean information about the high density behaviour of nuclear matter. Herein, the influence of modelling the pressure gradient by changing stiffness parameter and isospin asymmetry on the dynamics of charged particles have been investigated. In this research, three different values of stiffness parameter, $\gamma = 0.66$ (soft), 1 (stiff) and 2 (super-stiff), to tune the anisotropic transverse pressure gradients have been considered to explore the influence of density-dependent symmetry energy

$$E_{\mathrm{sym}}(\rho) = E_{\mathrm{sym}}(\rho_0)\left(\frac{\rho}{\rho_0}\right)^{\gamma}$$

on the electromagnetic field and energy density evolution. Stiffer symmetry energy ($\gamma = 2$) leads to larger pressure gradient than softer symmetry energy ($\gamma = 0.66$) that drives stronger expansion resulting in higher intensity of $(eB_y(0,0,0))_{\mathrm{max}}$ and $\langle|\mathbf{E}\cdot\mathbf{B}|\rangle_{\mathrm{max}}$. The correlation of eccentricity, nuclear stopping, centrality with the electromagnetic field and energy density have been established for different stiffness parameters. To deepen this study, the influence of isospin asymmetry (N/Z) on the time evolution of electromagnetic field has also been explored.

Keywords. Electromagnetic field; symmetry energy; nuclear stopping; eccentricity; rapidity; isospin quantum molecular dynamics.

PACS Nos **03.50.De; 41.20.−q; 25.70.−z; 25.75.Ld**

1. Introduction

Hydrodynamics [1,2], the heart of dynamical modelling, has widespread applications in studying the space-time evolution of highly dense nuclear matter during heavy-ion collisions (HICs). This highly dense nuclear matter results in an anisotropic pressure gradient [3,4] that generates compressional shock waves leading to various collective phenomena, such as sidewards deflection of nuclear matter in the reaction plane (i.e., side-splash) and azimuthal deflection of nuclear matter out of the reaction plane. Moreover, it gives insight about the crucial information regarding various other phenomena, such as nuclear stopping and electromagnetic field [5–12] of strongly interacting nuclear matter under the influence of various interactions like density-dependent symmetry energy [13–16], momentum-dependent interaction [17], Coulombic interaction [18], etc. The symmetry energy happens to be the most promising tool to study the isospin dependence of nuclear equation of state (NEOS). In recent years, many studies have been conducted on the isospin and density-dependent symmetry energy at sub-saturation density [15], anisotropic scaling [19,20], isospin diffusion [21,22], single and double ratios [23], isobaric ratio, etc. The anisotropic pressure due to the symmetry energy in asymmetric nuclear matter with an isospin asymmetry δ is expressed as [13]

$$P_{\mathrm{sym}} = (\rho^2 \partial E_{\mathrm{sym}}/\partial\rho)\delta^2, \tag{1}$$

where

$$E_{\mathrm{sym}}(\rho) = E_{\mathrm{sym}}(\rho_0)\left(\frac{\rho}{\rho_0}\right)^{\gamma}. \tag{2}$$

From the above equation, it has been observed that P_{sym} gradient can be tuned by varying the stiffness parameter

Published online: 13 December 2024

γ and isospin asymmetry δ. Pressure gradient influences the dynamics of nucleons and hence, it will be interesting to investigate the influence of γ and δ on the production of electromagnetic field.

Electromagnetic field is a class of meaningful observables which is capable of revealing the behaviour and the nature of the fiercely interacting medium developed by HICs. Experimentally, it was observed that Pb+Pb collision at 2.76 TeV/nucleon and Au+Au collisions at 200 GeV/nucleon generate magnetic field in the order of 10^{18}–10^{19} G [24]. Moreover, during HICs, simulation estimates that gigantic magnetic field can be generated in the order of 10^{18} G for extremely short time ($\approx 10^{-23}$ s). The high strength of the magnetic field has wide applications in the field of nuclear energy and defence sector. Therefore, research community is keenly interested in this field that can revolutionise the future. The potential of HICs to generate a very strong magnetic field is universally recognised [25–27]. As a result, the main focus of this study is on the evolution of electromagnetic field and $\langle|\mathbf{E}\cdot\mathbf{B}|\rangle_{\max}$ during HICs. Till now, the research community has taken great interest to study the effect of density-dependent symmetry energy on the collective flow and nuclear stopping. Hence, this work reports the effect of density-dependent symmetry energy on the generation of electromagnetic field and $\langle|\mathbf{E}\cdot\mathbf{B}|\rangle_{\max}$. This has not been reported to the best of our knowledge.

Further, to get reliable information about the evolution of electromagnetic field, knowledge regarding distribution of proton and neutron in the nucleus is highly necessary. Therefore, a very prominent and well-established isospin quantum molecular dynamics (IQMD) model [28] has been used to perform these simulations in which we need to replace Biot–Sawart law by Lineard–Wiechart potential. Hence, the aim of this study is four-fold, i.e.,

- To explore the influence of symmetry energy on the evolution of electromagnetic field.
- To investigate the effect of density-dependent symmetry energy on the production of $\langle|\mathbf{E}\cdot\mathbf{B}|\rangle_{\max}$.
- To study the correlation of electromagnetic field and $\langle|\mathbf{E}\cdot\mathbf{B}|\rangle_{\max}$ with the nuclear stopping.
- To study the influence of isospin asymmetry (N/Z) on the generation of electromagnetic field and $\langle|\mathbf{E}\cdot\mathbf{B}|\rangle_{\max}$.

2. Isospin quantum molecular dynamics model

IQMD model [28] is developed as an extension of quantum molecular dynamics (QMD) model [29]. The IQMD takes into account the isospin degree of freedom in a clear and distinct manner by incorporating the symmetry and Coulombic potential. Employing Monte Carlo sampling technique, IQMD accurately reproduces experimental data and contributes significantly to our understanding of nuclear matter under extreme conditions. The continuous refinement and application of IQMD continue to shed light on the intricate dynamics of nuclear system. This advance model also enables researchers to investigate the wide range of phenomena, such as multifragmentation, anisotropic flow, nuclear stopping and electromagnetic field evolution in the intermediate energy regime, where *n*–*n* interaction and mean-field potential contribute on equal footing in the dynamics of nucleons [30–33]. This model simulates the HICs in three essential steps, mainly,

(i) *Initialisation*
In the initialisation, Monte Carlo simulation has been employed to assign the coordinate and momentum to the nucleons associated with the target and the projectile. Coordinate and momentum of all these nucleons are assured within the sphere of radius $R = R_0 A^{1/3}$ (where A is the mass number) and momentum is restricted below the Fermi momentum $p \leq P_f$. In the first step, each nucleus is initialised by a Gaussian-shaped density distribution wave packet and the distribution of all nucleons is represented by

$$f_i(\mathbf{r},\mathbf{p},t) = \frac{1}{\pi^2\hbar^2} \mathrm{e}^{-(\mathbf{r}-\mathbf{r_i}(t))^2 \frac{1}{2L}} \times \mathrm{e}^{-(\mathbf{p}-\mathbf{p_i}(t))^2 \frac{2L}{\hbar^2}}, \tag{3}$$

where $\mathbf{r_i}(t)$ and $\mathbf{p_i}(t)$ are the mean position and momentum of the ith nucleon at time t. The interaction range of each nucleon is characterised by the Gaussian width ($L = 8.66$ fm^2 for Au+Au collision) which is system's size-dependent, ensuring that the nucleus achieves maximum stability.

(ii) *Propagation*
After the initialisation, the nuclei of the target and the projectile are accelerated towards each other, ensuring that the centre of mass energy is maintained properly. The IQMD model employs Hamilton equations of motion to describe the position and momentum of the nucleons in an interaction potential:

$$\frac{\mathrm{d}\mathbf{r_i}}{\mathrm{d}t} = \frac{\mathrm{d}\langle H\rangle}{\mathrm{d}\mathbf{p_i}}, \quad \frac{\mathrm{d}\mathbf{p_i}}{\mathrm{d}t} = -\frac{\mathrm{d}\langle H\rangle}{\mathrm{d}\mathbf{r_i}}, \tag{4}$$

where

$$\langle H\rangle = \langle T\rangle + \langle V\rangle$$
$$= \sum_i \frac{p_i^2}{2m_i} + \sum_i \sum_{j>i} \int f_i(\mathbf{r},\mathbf{p},t) V_{ij} \times (\mathbf{r}',\mathbf{r}) f_j(\mathbf{r}',\mathbf{p}',t)\mathrm{d}\mathbf{r}\,\mathrm{d}\mathbf{r}'\,\mathrm{d}\mathbf{p}\,\mathrm{d}\mathbf{p}'. \quad (5)$$

Here, V_{ij}, the total nucleon–nucleon potential, is the sum of Skyrme interaction, Yukawa potential, Coulomb interaction as well as symmetry potential.

$$V_{ij}(\mathbf{r}'-\mathbf{r}) = V_{ij}^{\text{Skyrme}} + V_{ij}^{\text{Yukawa}} + V_{ij}^{\text{Coul}} + V_{ij}^{\text{MDI}} + V_{ij}^{\text{Sym}}$$
$$= \left(t_1\delta(\mathbf{r}'-\mathbf{r}) + t_2\delta(\mathbf{r}'-\mathbf{r})\rho^{\zeta-1}\left(\frac{\mathbf{r}'+\mathbf{r}}{2}\right)\right) + t_3\frac{\exp(|\mathbf{r}'-\mathbf{r}|/\mu)}{(|\mathbf{r}'-\mathbf{r}|/\mu)} + \frac{Z_iZ_j\mathrm{e}^2}{|\mathbf{r}'-\mathbf{r}|} + t_4\ln^2[t_5(\mathbf{p}'-\mathbf{p})^2+1]\delta(\mathbf{r}'-\mathbf{r}) + t_6\frac{1}{\varrho_0}T_{3i}T_{3j}\delta(\mathbf{r}'-\mathbf{r}). \quad (6)$$

In the present scenario, Z_i and Z_j represent the charges of the ith and jth baryons, while T_{3i} and T_{3j} correspond to their respective T_3 components. The parameters μ (= 0.4 fm) and t_1, $t_2,\ldots,t_6$ have been adjusted to accurately represent the real part of the nucleonic optical potential [34–36]. Within the context of IQMD model, symmetry energy can be expressed as a function of density. At normal nuclear matter, magnitude of symmetry energy is taken as 32.0 MeV.

$$E_{\text{sym}}(\rho) = 32\times\left(\frac{\rho}{\rho_0}\right)^{\gamma}\ \text{MeV}. \quad (7)$$

The term gamma (γ) has been used to quantify the magnitude of the symmetry energy. More details of the model has been reported elsewhere [36].

(iii) *n–n collision*
In the final stage, collision term is employed to describe the interaction between two nucleons when the minimum distance between nucleon's centroid is less than $\sqrt{\sigma_{\text{tot}}/\pi}$ and binary collision among them become prominent in interaction dynamics. Furthermore, the consideration of Pauli blocking has been taken into account to examine the phase-space densities in the aforementioned states.

For investigating the evolution of electromagnetic field during HICs, the integration of electromagnetic field into the transport model is accomplished by introducing Lienard-Wiechert potentials [27].

$$e\mathbf{B}(\mathbf{r},t) = \frac{\mathrm{e}^2}{4\pi\epsilon_0 c}\sum_n Z_n \frac{c^2-v_n^2}{(cR_n-\boldsymbol{R}_n\cdot\boldsymbol{v}_n)^3}(\boldsymbol{v}_n\times\boldsymbol{R}_n) \quad (8)$$

$$e\mathbf{E}(\mathbf{r},t) = \frac{\mathrm{e}^2}{4\pi\epsilon_0 c}\sum_n Z_n \frac{c^2-v_n^2}{(cR_n-\boldsymbol{R}_n\cdot\boldsymbol{v}_n)^3} \times(c\boldsymbol{R}_n - \boldsymbol{R}_n\mathbf{v}_n). \quad (9)$$

When $\boldsymbol{v}_n \ll$ c, the above equation turns into

$$e\mathbf{B}(\mathbf{r},t) = \frac{\mathrm{e}^2}{4\pi\epsilon_0 c^2}\sum_n Z_n\frac{1}{R_n^3}(\boldsymbol{v}_n\times\boldsymbol{R}_n), \quad (10)$$

$$e\mathbf{E}(\mathbf{r},t) = \frac{\mathrm{e}^2}{4\pi\epsilon_0 c^2}\sum_n Z_n\frac{1}{R_n^3}\mathbf{R}_n, \quad (11)$$

where Z_n is the charge number of the nth particle, $\mathbf{R}_n = \mathbf{r}-\mathbf{r}'_n$ is the relative position of the field point $\mathbf{r}$ to the nth particle's source point $\mathbf{r}'_n$ and $\mathbf{v}_n$ is the velocity of the nth particle at the retarded time $t_{rn} = t - |\mathbf{r}-\mathbf{r}'_n(t_{rn})|/c$. It should be noted that these equations have singularities at $R_n = 0$. To mitigate the singularities and self-interaction effects, particles within a Lorentz-contracted cell are selectively excluded from electromagnetic field calculations. Energy transfer from the participant to the spectator zones induces magnetic field generation, altering charged particle velocities in the spectator zone. This approach has been refined through various regularisation procedures to obtain reliable results.

3. Results and discussion

This work concentrates on the effect of density-dependent symmetry energy and isospin asymmetry on various observables, such as magnetic field, electric field and energy density generated during HIC. In this work, studies have been carried out by simulating thousands of events in *n–n* reference frame for the Au+Au collisions at an incident energy of 500 MeV/nucleon. For this, the symmetry energy is varied by using different values of stiffness parameter, i.e., $\gamma = 0.66$, 1 and 2 as well as by changing the N/Z ratio. The position and momentum of the particles as a function of time have been simulated using the IQMD model. In the initial stage of the collisions, explosive collective flow begins before the matter reaches equilibrium.

During HIC, an almond-shaped region is inhabited by the participant matter. The region beyond this almond-shaped zone corresponds to the spectator zone that is the predominant source of electromagnetic field [32,33]. The magnetic field in HICs originates from the collective contribution of the moving charged nucleons.

Notably, in the IQMD model, participant and spectator nucleon categorisations are not based on the geometric consideration, but rather dynamics interactions, adding a nuanced dimension to nuclear reaction simulations.

During HIC, the pressure gradient P_{sym} can be modelled by changing stiffness parameter [13] and isospin asymmetry [37–42]. Therefore, it is necessary to explore its impact on the production of electromagnetic field during HICs.

Figure 1a demonstrates the progression of magnetic field $eB_y(0, 0, 0)$ with time at a particular scaled impact parameter with a colliding energy of 500 MeV/nucleon. This variation has been observed for different density-dependent symmetry energy by taking various stiffness parameter values, $\gamma = 0.66$, 1 and 2. It is worth noting that the in-plane momentum of the charged nucleon during HICs contributes significantly in the evolution of magnetic field in the y-direction. Besides, the generation of magnetic field is influenced by the transfer of energy from the participant to the spectator zone which leads to the change in velocity of the charged particles of the spectator zone. Initially, when two nuclei collide relativistically, the magnetic field increases very sharply due to large change in velocity of the charged particles. And the magnetic field intensity reaches at its apex value during the utmost compression of the nuclei [32]. After that, magnetic field intensity starts decreasing when the nuclear matter moves apart from each other and therefore, transfer of energy will stop [27,32].

Further, the fire ball zone (i.e., the compressed nuclear matter) or the pressure gradient in highly compressed zone can be varied by taking different values of γ [13, 16]. The stiffness of the symmetry energy reflects the rate at which the density of the overlapping zone changes with energy. It was observed that the stiffness parameter, $\gamma = 2$, results in larger momentum of charged nucleons than the lower stiffness parameter value [16].

Hence, the maximum value of the magnetic field intensity will be smaller for $\gamma = 0.66$ than the hardest stiffness parameter ($\gamma = 1, 2$). In other words, higher value of γ associated with a stiffer symmetry energy resulted in more kinetic energy for the neutron-rich matter in $^{197}_{79}\text{Au} + ^{197}_{79}\text{Au}$ collision [13,15,16,43]. As a result, stronger repulsive forces between nucleons are observed and this contributes to higher magnetic field intensity for the nucleons involved in the collision with stiffer symmetry energy. Conversely, a softer symmetry energy, characterised by a lower stiffness parameter value, corresponds to a slower increase in kinetic energy with density for neutron-rich matter [15]. This can lead to weaker repulsion between nucleons, potentially resulting in a lower magnetic field intensity.

Likewise, the variation of electric field at the central point, i.e., $eE_y(0, 0, 0)$ with time is shown in figure 1b by taking other parameter the same. Herein, the squeezed-out nucleons during HICs play a dominant role for the production of electric field in the y-direction. Interestingly, the flow of electric field intensity with time will follow the same pattern with different magnitude as the magnetic field. But for the super-stiffer ($\gamma = 2$) symmetry energy term, expansion of nucleon will be higher. Therefore, the maximum electric field intensity is higher for super-stiffness symmetry energy ($\gamma = 2$) than for softer symmetry energy.

To gain deep insights, the temporal evolution of the electromagnetic field at a spatial point (0, 1, 0) has been studied. Figure 2 demonstrates that the pattern adhered by the magnetic and electric field evolutions at the off-central point ($eB_y(0, 1, 0)$, $eE_y(0, 1, 0)$) is almost similar as displayed for the central point (0, 0, 0). Nevertheless, a decrement in the intensity of the electromagnetic field at the off-central point (0, 1, 0) can be seen in figures 2a and 2b, that is in good agreement with the results reported in [26].

Intensity of the magnetic field generated during HIC gets its maximum strength for a very short interval of time and therefore the effect of density-dependent symmetry energy as well as interaction zone between the nuclei on maximum intensity of the magnetic field $(eB_y(0, 0, 0))_{\text{max}}$ and electric field $(eE_y(0, 0, 0))_{\text{max}}$ has been explored. The effect of symmetry energy on $(eB_y(0, 0, 0))_{\text{max}}$ for various impact parameters is depicted in figure 3a. It has been observed that $(eB_y(0, 0, 0))_{\text{max}}$ increases as the impact parameter becomes larger. This is due to the symmetric distribution of nucleons and maximum stopping at low impact parameters resulting into a smaller intensity of $(eB_y(0, 0, 0))_{\text{max}}$. Furthermore, at very low impact parameter (i.e., $b/b_{\text{max}} = 0.1$), the effect of stiffness parameter is very minimal due to very less number of charged nucleons participating in the generation $eB_y(0, 0, 0)$. The squeezing of nucleons will be maximum at very low impact parameter and contribution of these squeezed nucleons in the evolution of the magnetic field in the y-direction is very minimal. Therefore, no significant effect was observed in the magnitude of $(eB_y(0, 0, 0))_{\text{max}}$ for different stiffness parameters at low impact parameter. Afterwards, the effect of density-dependent symmetry energy starts becoming significant as we increase the impact parameter due to increase in spectator zone (decrease in nuclear stopping). This may be because the transfer of energy from the participant to the spectator zone becomes significant for various stiffness parameters resulting in different pressure gradients. But, at semiperipheral collisions ($b/b_{\text{max}} = 0.7$), this density-dependent symmetry energy effect becomes insignificant due to the small participant zone. Therefore, transfer of energy due to the change in pressure

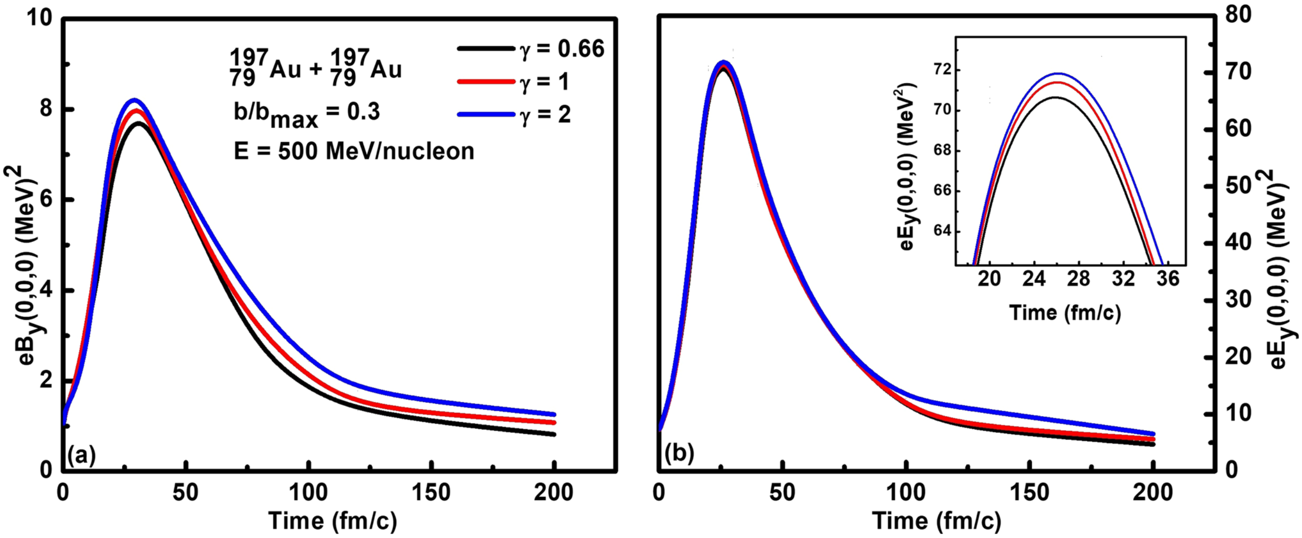

Figure 1. Time evolution of (**a**) $eB_y(0, 0, 0)$ and (**b**) $eE_y(0, 0, 0)$ at $b/b_{\max} = 0.3$ when the colliding energy is 500 MeV/nucleon for various stiffness parameter values.

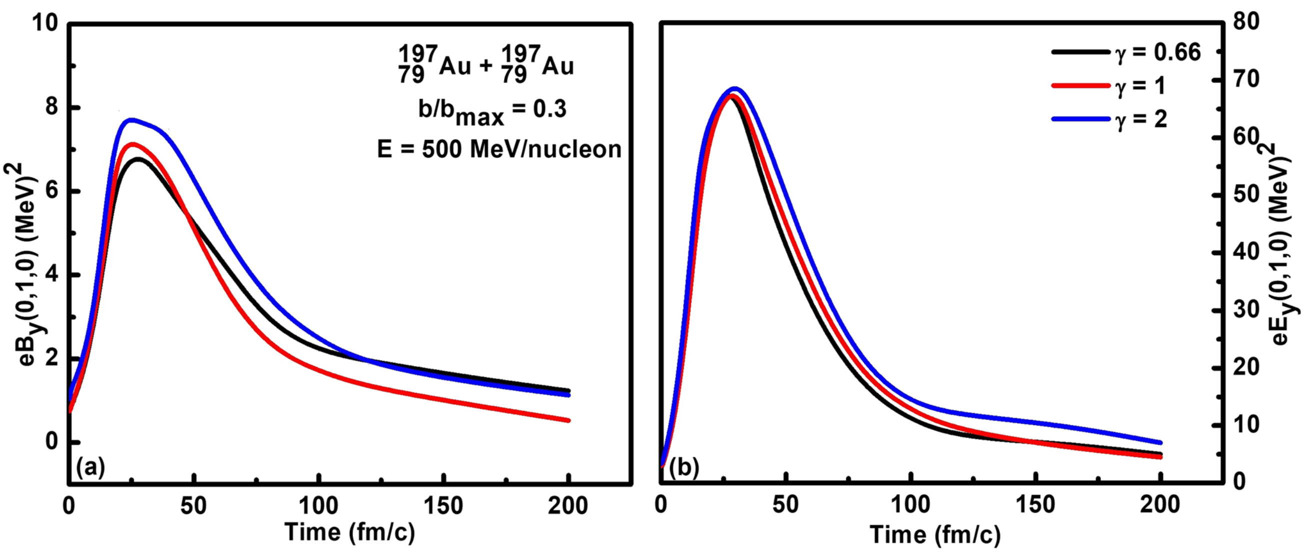

Figure 2. Temporal evolution of (**a**) $eB_y(0, 1, 0)$ and (**b**) $eE_y(0, 1, 0)$ at $b/b_{\max} = 0.3$ when the colliding energy is 500 MeV/nucleon for various stiffness parameter values.

gradient can be altered when the change in γ is minimal. Thus, it can be clearly seen that the effect of stiffness parameter is most significant at $b/b_{\max} = 0.5$. The same study has been performed for the electric field in the y-direction and it was observed that the trend followed by the electric field is inverse to the trend followed by the magnetic field. Figure 3b shows that intensity of $(eE_y(0, 0, 0))_{\max}$ slightly increases with the impact parameter and then starts decreasing as we further move towards higher impact parameter due to a decrease in the participant zone. This is because at the low impact parameter, squeeze-out of nucleons will be more which contributes significantly in the generation of $(eE_y(0, 0, 0))$. The squeeze-out of nucleons decreases for higher impact parameter leading to the reduction in the intensity of the electric field in the y-direction. Moreover, no significant effect has been observed for the scaling of electric field with impact parameter by taking different values of stiffness parameter. However, a little variation in the intensity for different values of γ has been observed near semi-central collision at which maximum squeezing of nucleons takes place.

Moreover, the variation of maximum intensity of the electromagnetic field with impact parameter at the off-central point (0, 1, 0) has also been demonstrated in

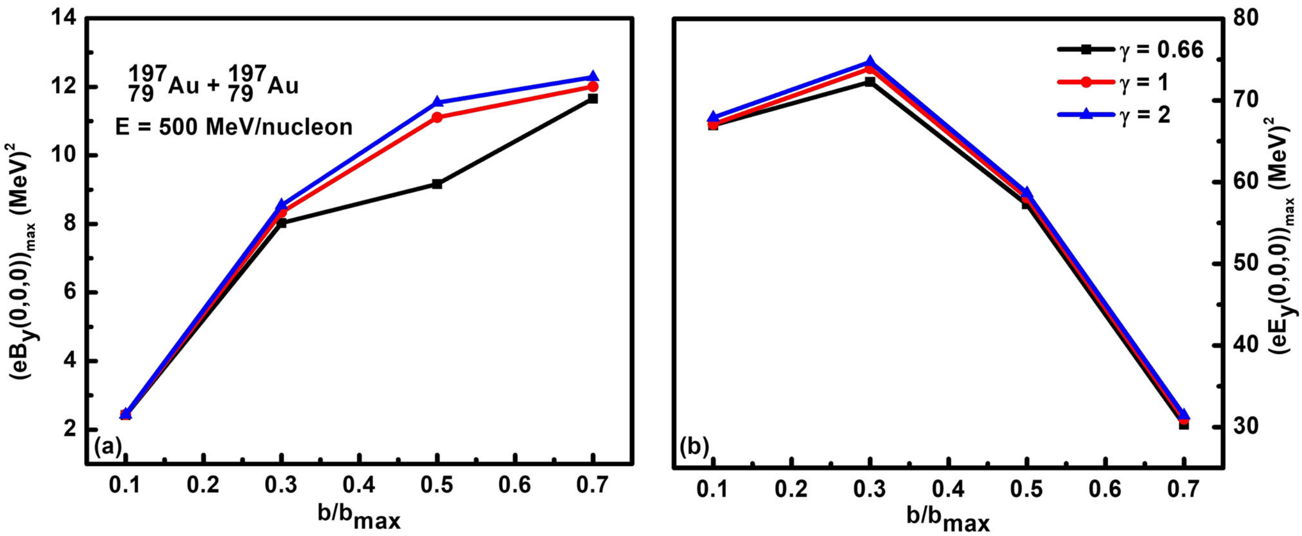

Figure 3. The variation of (**a**) $(eB_y(0,0,0))_{\max}$ and (**b**) $(eE_y(0,0,0))_{\max}$ with scaled impact parameter at 500 MeV/nucleon for $\gamma = 0.66$, 1 and 2.

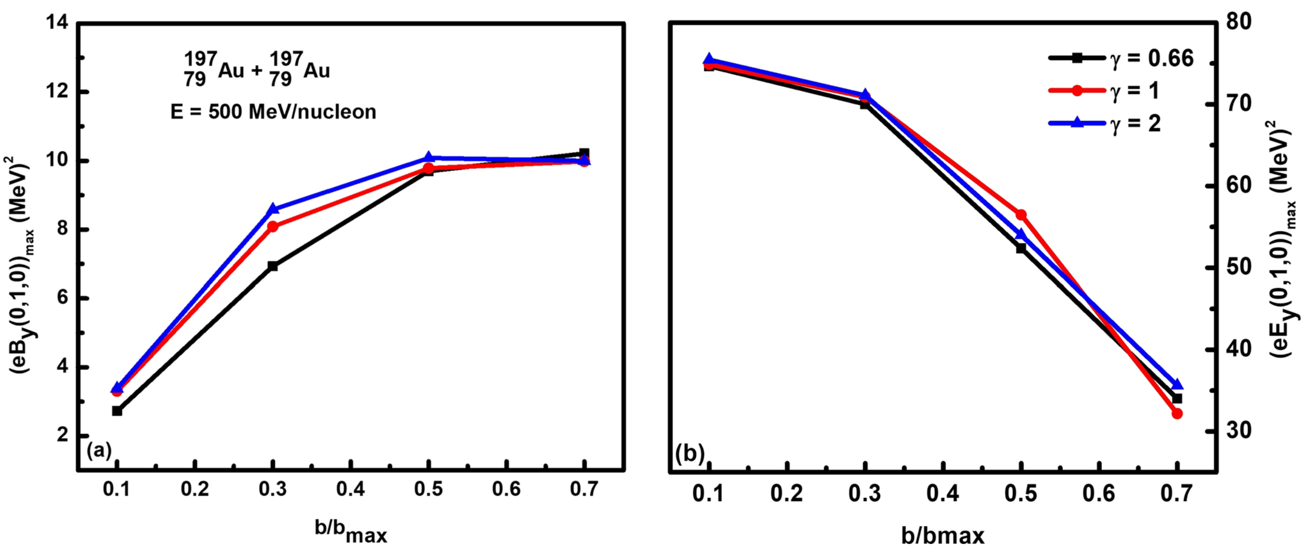

Figure 4. The variation of (**a**) $(eB_y(0,1,0))_{\max}$ and (**b**) $(eE_y(0,1,0))_{\max}$ with the scaled impact parameter at 500 MeV/nucleon for $\gamma = 0.66$, 1 and 2.

figures 4a and 4b. Figure 4a shows that $(eB_y(0,1,0))_{\max}$ increases and then saturates with the increase in impact parameter at the off-central point also but with a marginal decrease in its intensity compared to the central point (0, 0, 0) at higher values of impact parameter. Figure 4b shows that $(eE_y(0,1,0))_{\max}$ consistently decreases as the impact parameter increases for different values of γ.

Further, the formation of anisotropic pressure gradient zone will be highly dependent on γ. Therefore, to investigate the effect of γ on the flow of nucleons, the eccentricity of the participant zone becomes necessary. Additionally, the overlapping zone for each event does not conform strictly to an almond shape, often exhibiting deviations in the orientation of its shorter axis with respect to the impact parameter direction. These variations in shape and direction are aptly captured by the eccentricity parameter. Participant eccentricity emerged as the critical geometric parameter responsible for generating the azimuthal asymmetry that underlines the observed flow phenomena. The eccentricity of the participant zone indicates its elongation or deformation along a specific direction. Therefore, investigating the consequences of symmetry energy on the eccentricity

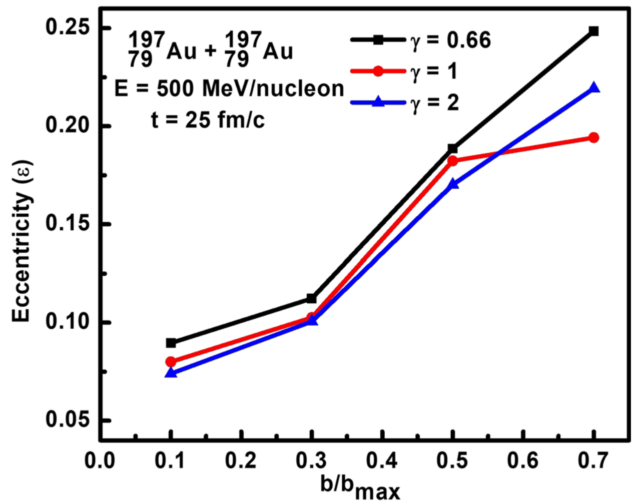

Figure 5. Variation of participant eccentricity with scaled impact parameter when the colliding energy is 500 MeV/nucleon for different values of γ.

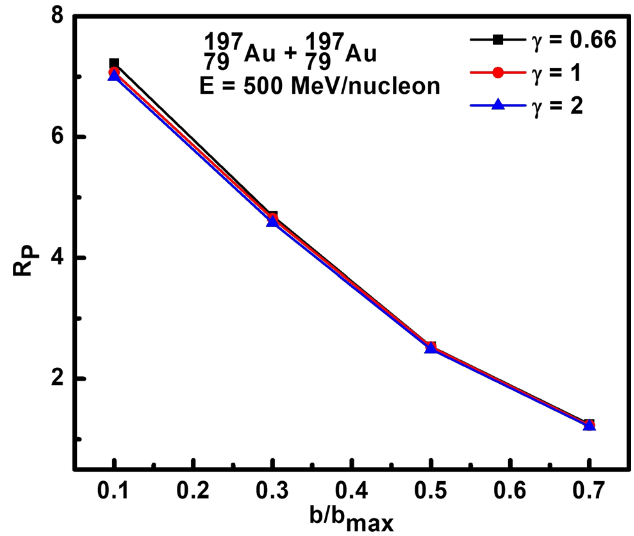

Figure 6. Impact parameter dependence of nuclear stopping for $\gamma = 0.66$, 1 and 2 at 500 MeV/nucleon.

provides qualitatively new insight about the initial conditions of HICs and the subsequent collective expansion of the system. Figure 5 shows the variation of eccentricity of the participant zone in the x–y plane with the scaled impact parameter by taking $\gamma = 0.66$, 1 and 2. The spatial eccentricity [44–46] in the x–y plane can be described as

$$\langle \epsilon_{\text{part}} \rangle = \frac{\langle y^2 - x^2 \rangle}{\langle y^2 + x^2 \rangle}. \tag{12}$$

It was found that the value of eccentricity in the x–y plane increases with the rise in scaled impact parameter value (figure 5). This is assigned to the decrease in semi-major axis of elliptical flow with increase in centrality. Furthermore, when the symmetry energy is stiffer, characterised by a higher stiffness parameter, the repulsive forces between nucleons become stronger. This leads to a greater resistance to the compression and expansion of the participant zone, resulting in a less deformed and more compact shape. Consequently, the magnitude of eccentricity for the stiffer symmetry energy ($\gamma = 2$) is smaller than that of the softer symmetry energy ($\gamma =$ 0.66 and 1). A softer symmetry energy as defined by a lower stiffness value, leads to a reduced repulsion between nucleons. This allows for a more expanded and deformed participant zone, resulting in a larger eccentricity.

Moreover, the nuclear stopping tells us about the dissipation of longitudinal energy that is highly dependent on the centrality of the overlapping region. The highly dense overlap region plays an important role in nuclear stopping. Therefore, figure 6 showcases the fluctuation of nuclear stopping with the scaled impact parameter for $\gamma = 0.66$, 1 and 2. It can be clearly seen from figure 6 that as the impact parameter increases, nuclear stopping diminishes. When the impact parameter is small which corresponds to the central collision with an extensive overlap region, the nucleons from both nuclei engage more frequently and experience a higher degree of stopping. This is a consequence of a higher probability of nucleon-nucleon collisions and entailed energy transfer between the colliding nuclei. As a result, the forward momentum of the nucleons decreases more effectively, resulting in greater nuclear stopping (figure 6). However, as the impact parameter increases, the overlap region between the colliding nuclei shrinks and fewer nucleon-nucleon interactions occur. As a result, the nucleons have a lesser probability of transferring energy and momentum to one another, leading to lesser nuclear stopping. Consequently, the forward momentum of the nucleons is less effectively reduced for the collisions occurring at higher impact parameters. The dependency of nuclear stopping on the stiffness parameter of the symmetry energy sheds light on the fundamental mechanism of driving collision dynamics and the properties of nuclear matter. Therefore, it is important to investigate the variation of nuclear stopping in HICs with varying stiffness parameters of the symmetry energy. In general, a stiffer symmetry energy results in greater repulsion between nucleons which alters the collision dynamics resulting in a changed pattern of energy transfer and nuclear stopping. According to this study, at a lower impact parameter, nuclear stopping is generally lower in collisions involving nuclei with stiffer symmetry energy than collisions involving nuclei with softer symmetry energy. This can be attributed to the enhanced repulsive forces between nucleons which reduces the degree of energy transfer and momentum exchange. This is because softer symmetry energy allows for a greater degree of interaction between the nucleons, leading to later emission with enhanced collision probabilities [43]. In other words, one can say that soft symmetry energy may tend to induce more nucleon-nucleon collisions and hard symmetry energy may tend to minimise the collisions.

Further investigation of electromagnetic field with some other observables gives more insight to enhance the understanding about the contribution of nucleons to generate the magnetic and electric fields. Figure 7a shows the correlation of the evolution of $(eB_y(0, 0, 0))_{\max}$ and the nuclear stopping and its comparison for different stiffness parameter values. The out-of-plane emission will be more with the increase in nuclear stopping while the spectator nucleons will be lesser. The production of magnetic field in the y-direction is mainly due to the spectator nucleons and therefore, it decrease with increase in nuclear stopping. Moreover, in the case of stiffer symmetry energy ($\gamma = 2$), highly anisotropic pressure gradient will be developed compared to softened energy ($\gamma = 0.66$) [43]. The repulsive interactions between the nucleons are higher in collisions involving nuclei with a stiffer symmetry energy, leading to the exhibition of more kinetic energy in the nucleons during the HICs process [43]. As the nucleons engage and move away from each other during the collision, the increased repulsion can result in more energetic nucleons. Therefore, acceleration of nucleons will be higher for $\gamma = 2$, resulting in large magnetic field $(eB_y(0, 0, 0))_{\max}$ for hardened symmetry energy. Likewise, the variation of $(eE_y(0, 0, 0))_{\max}$ with nuclear stopping for various stiffness parameters has been demonstrated in figure 7b. Initially, the intensity of $(eE_y(0, 0, 0))_{\max}$ rises to attain its zenith and starts decreasing afterwards with the nuclear stopping, because the increased nuclear stopping leads to more squeeze-out of nucleons contributing in the generation of electric field in the y-direction.

The combination of the electric field ($\mathbf{E}$) with the magnetic field ($\mathbf{B}$) transforms into the Lorentzian invariant $\mathbf{E} \cdot \mathbf{B}$ that reverses its sign under parity transformation [12]. The space-time distribution of energy density of the charged nucleons is an important parameter to study. The generation of $\mathbf{E} \cdot \mathbf{B}$ during HIC is directly correlated with the temperature and density of the overlapping zone. Therefore, it is meaningful to explore the effect of density-dependent symmetry energy on time evolution of $\mathbf{E} \cdot \mathbf{B}$. Figure 8a displays the variation of $\langle|\mathbf{E} \cdot \mathbf{B}|\rangle$ with time for different stiffness parameters. $\langle|\mathbf{E} \cdot \mathbf{B}|\rangle$ steeply rises to attain its maximum value and starts decreasing slowly. It is worth mentioning that the energy density attains its maximum value in the highly compressed zone of the colliding nuclei (approximate at 30 fm/c).

Further, it is also worth considering that the impact of γ is almost invisible before the maximum compressional zone is created, but it becomes significant after that. The rate of change of $\langle|\mathbf{E} \cdot \mathbf{B}|\rangle$ is very high before the maximum compressional zone that neglects the effect of stiffness parameter. The effect of density-dependent symmetry energy becomes visible after the maximum compression zone because most of the energy transfer takes place in this region. Moreover, in the case of super-stiffer symmetry energy term, transfer of energy will be more due to lesser nuclear stopping resulting in higher value of $\langle|\mathbf{E} \cdot \mathbf{B}|\rangle$. Further, the variation of $\langle|\mathbf{E} \cdot \mathbf{B}|\rangle_{\max}$ with the scaled impact parameter has been evaluated in figure 8b. It has been observed that the value of $\langle|\mathbf{E} \cdot \mathbf{B}|\rangle_{\max}$ decreases with the increase in the scaled impact parameter. This is mainly attributed to the fact that more energy is transferred at the lower impact parameter resulting in the evolution of more energy density value.

Till now, the effect of symmetry energy and its density dependence on the electromagnetic field and $\langle|\mathbf{E} \cdot \mathbf{B}|\rangle$ have been studied by taking fixed ratio of proton and neutron, i.e., $N/Z = 1.4$. However, it has been noticed that the symmetry energy increases with the increase in N/Z ratio. Therefore, this study has been extended to study the role of isospin as well as system size by taking the isotopic series of ${}_{50}\mathrm{Sn}_X + {}_{50}\mathrm{Sn}_X$, where $X = 62, 68, 74$. It can be noticed from eqs (5) and (6) that the electric and magnetic fields depend upon the number of protons. So, the number of protons has been kept fixed for various values of N/Z. Figure 9a demonstrates the variation of energy density with time for different values of N/Z. Mainly two factors, i.e., isospin effect and system size effect, are responsible for the variation in energy density. The energy density rises very sharply at the initial stage and reaches its maximum value. After that, it gradually starts decreasing with time. Moreover, the maximum value of energy density is larger for higher N/Z ratio than for lower N/Z ratio.

Further, figure 9b shows the variation of $\langle|\mathbf{E} \cdot \mathbf{B}|\rangle_{\max}$ with the scaled impact parameter for different values of N/Z. The maximum value of energy density decreases with the increase in impact parameter while the change is observed due to different N/Z values at lower impact parameters. It can be concluded that stiffness parameter γ and isospin asymmetry modelled the pressure gradient of the overlapping region in a significant way. The tuning of pressure gradient leads to changes in the dynamics of the charged nucleons. Further, it was observed that the modelling of the dynamics of nucleons affect the production of electromagnetic field and $\langle|\mathbf{E} \cdot \mathbf{B}|\rangle_{\max}$ in

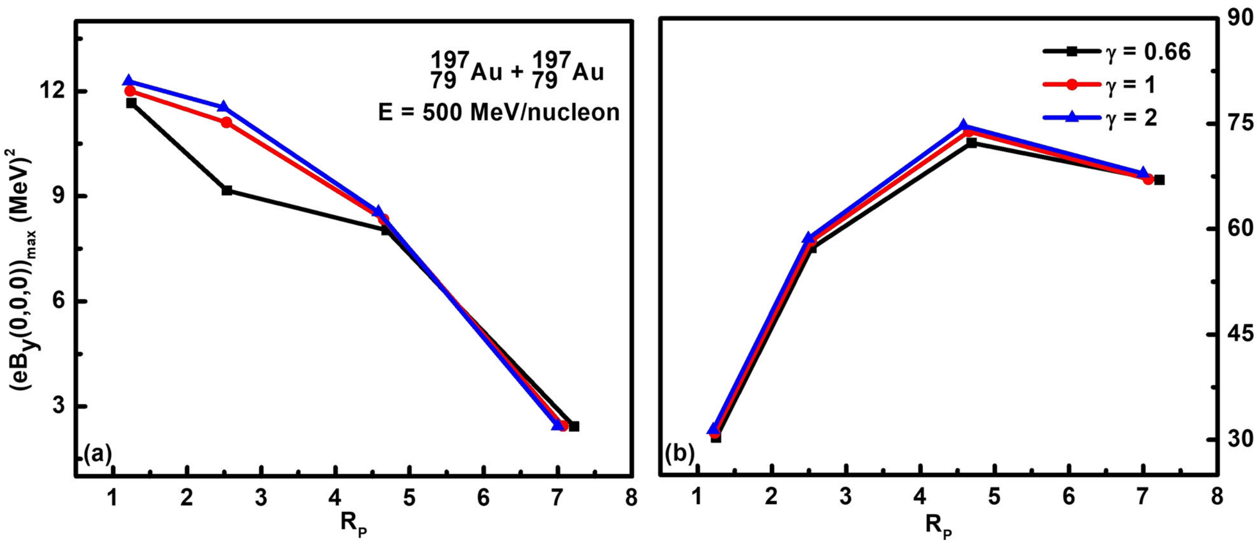

Figure 7. Correlation between (**a**) $(eB_y(0,0,0))_{\max}$ and (**b**) $(eE_y(0,0,0))_{\max}$ with nuclear stopping for $\gamma = 0.66$, 1 and 2 at 500 MeV/nucleon.

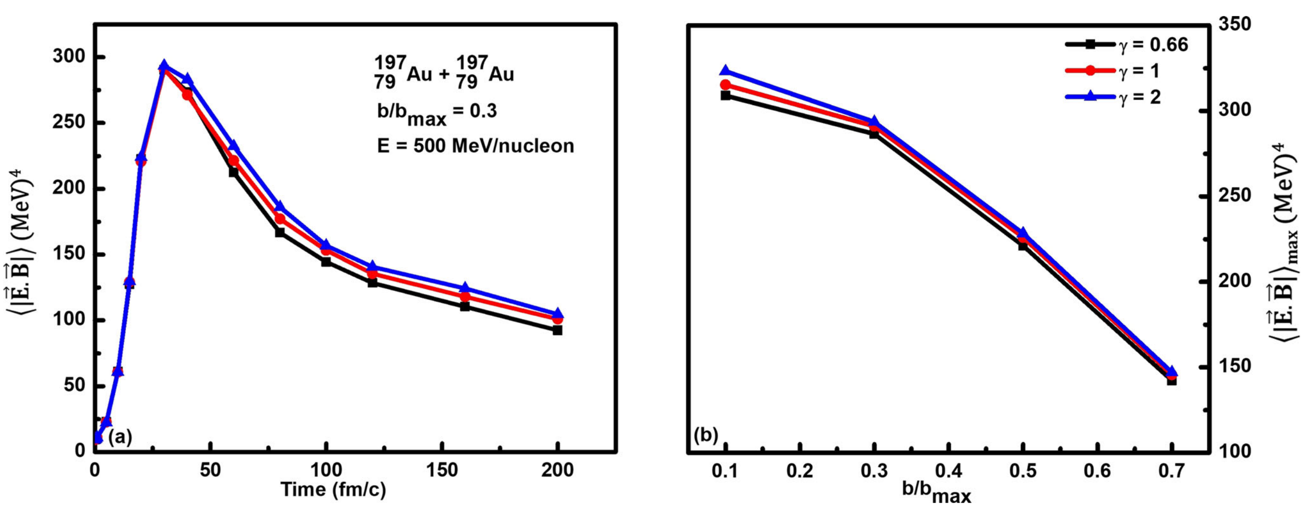

Figure 8. (**a**) Time evolution of $\langle|\mathbf{E}\cdot\mathbf{B}|\rangle$ at $b/b_{\max} = 0.3$ for 500 MeV/nucleon colliding energy for different stiffness parameter values and (**b**) variation of $\langle|\mathbf{E}\cdot\mathbf{B}|\rangle_{\max}$ with scaled impact parameter at 500 MeV/nucleon colliding energy for different symmetry energy stiffness parameter values ($\gamma = 0.66$, 1 and 2).

a significant manner. The intensities of $eB_y(0,0,0)$ and $eE_y(0,0,0)$ are the highest for the super-stiffer symmetry energy ($\gamma = 2$). Moreover, it was noted that the influence of symmetry energy is more visible due to maximum compression. Likewise, the influence of isospin symmetry has been explored by taking isotopic series of ${}_{50}\mathrm{Sn}_X + {}_{50}\mathrm{Sn}_X$, where $X = 62, 68, 74$. It has been observed that the intensity of $\langle|\mathbf{E}\cdot\mathbf{B}|\rangle$ is higher for higher N/Z ratio and, is much more significant at lower impact parameter than at higher impact parameter. Figures 9a and 9b show that the maximum value of energy density increases with increase in N/Z value while it was already discussed in figures 8a and 8b that $\langle|\mathbf{E}\cdot\mathbf{B}|\rangle_{\max}$ also increases with increase in the stiffness parameter. Thus, both these parameters influence the reaction dynamics in the same manner.

4. Conclusion

In summary, the variation of density-dependent symmetry energy and isospin asymmetry modelled the pressure gradient of the overlapping region in a significant way. This tuning of pressure gradient leads to a change in the dynamics of charged nucleons which in turn affects the production of electromagnetic field and

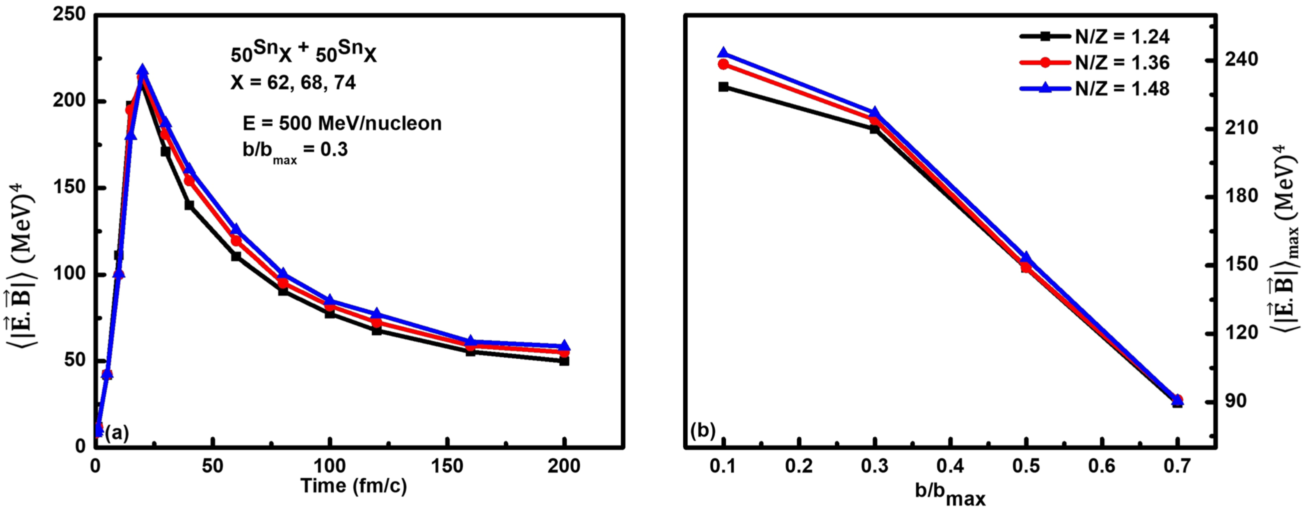

Figure 9. (**a**) Time evolution of $\langle|\mathbf{E}\cdot\mathbf{B}|\rangle$ at $b/b_{\max} = 0.3$ for 500 MeV/nucleon colliding energy for different N/Z ratios and (**b**) variation of $\langle|\mathbf{E}\cdot\mathbf{B}|\rangle_{\max}$ with scaled impact parameter at 500 MeV/nucleon colliding energy for different N/Z ratios.

energy density remarkably. The obtained result reveals significant variations in the generated electromagnetic field as a function of the stiffness parameter of the symmetry energy. The intensities of $(eB_y(0,0,0))_{\max}$ and $\langle|\mathbf{E}\cdot\mathbf{B}|\rangle_{\max}$ are the highest for the super-stiff symmetry energy. Moreover, it was observed that the influence of symmetry energy is more visible after the time of maximum compression. Likewise, the influence of isospin asymmetry has been explored by taking isotopic series of $_{50}\mathrm{Sn}_X +_{50}\mathrm{Sn}_X$ where $X = 62, 68, 74$. It was found that the intensity of energy density is higher for higher N/Z ratio.

Acknowledgement

The authors extend their sincere appreciation to R K Puri for his generous provision of access to his computer code and for his participation in insightful and productive discussions.

References

[1] A Jaiswal and V Roy, *Adv. High Energy Phys.* **1**, 9623034 (2016)
[2] C Shen and L Yan, *Nucl. Sci. Technol.* **31(12)**, 122 (2020)
[3] M Demoulins *et al*, *Phys. Lett. B* **241**, 476 (1990)
[4] H Gutbrod *et al*, *Phys. Lett. B* **216**, 267 (1989)
[5] K Tuchin, *Phys. Rev. C* **88**, 024911 (2013)
[6] D E Kharzeev, L D McLerran and H J Warringa, *Nucl. Phys. A* **803**, 227 (2008)
[7] A Bzdak and V Skokov, *Phys. Lett. B* **710**, 171 (2012)
[8] E Stewart and K Tuchin, *Nucl. Phys. A* **1016**, 122308 (2021)
[9] G Inghirami *et al*, *Eur. Phys. J. C* **80(3)**, 1 (2020)
[10] D E Kharzeev and J Liao, *Nat. Rev. Phys.* **3(1)**, 55 (2021)
[11] G F Wei *et al*, *Phys. Rev. C* **98(2)**, 024618 (2018)
[12] V Voronyuk *et al*, *Phys. Rev. C* **83(5)**, 054911 (2011)
[13] L W Chen *et al*, *Phys. Rev. Lett.* **90(16)**, 162701 (2003)
[14] K S Vinayak and S Kumar, *J. Phys. G: Nucl. Part. Phys.* **39(9)**, 095105 (2012)
[15] S Kumar *et al*, *Phys. Rev. C* **84(4)**, 044620 (2011)
[16] G Yong, *Phys. Lett. B* **786**, 422 (2018)
[17] J Aichelin *et al*, *Phys. Rev. Lett.* **58(19)**, 1926 (1987)
[18] V Y Denisov, *Phys. Lett. B* **526(3–4)**, 315 (2002)
[19] J Noronha-Hostler and M Gyulass, *Phys. Rev. C* **93(2)**, 024909 (2016)
[20] T Z Yan and S Li, *Chin. Phys. C* **38(8)**, 084104 (2014)
[21] L W Chen, C M Ko and B A Li, *Phys. Rev. Lett.* **94(3)**, 032701 (2005)
[22] A Camaian *et al*, *Phys. Rev. C* **103(1)**, 014605 (2021)
[23] S Kumar, Y G Ma and G Q Zhang, *Phys. Rev. C* **84(4)**, 044620 (2011)
[24] B X Chen and S Q Feng, *Chin. Phys. C* **44(2)**, 024104 (2020)
[25] XL Zhao *et al*, *Phys. Lett. B* **792**, 413 (2019)
[26] J Bloczynski *et al*, *Phys. Lett. B* **718(4–5)**, 1529 (2013)
[27] O Li and B A Li, *Phys. Rev. C* **84(6)**, 064605 (2011)
[28] C Hartnack *et al*, *Eur. Phys. J. A* **1(2)**, 151 (1998)
[29] J Aichelin, *Phys. Rep.* **202(5–6)**, 233 (1991)
[30] Y X Zhang *et al*, *Front. Phys.* **15(5)**, 1 (2020)
[31] Y J Wang and Q F Li, *Front. Phys.* **15(4)**, 1 (2020)
[32] D Sharma and S Kumar, *J. Phys. G: Nucl. Part. Phys.* **50(4)**, 045109 (2023)
[33] D Sharma and S Kumar, *J. Phys. G: Nucl. Part. Phys.* **51**, 055102 (2024)
[34] L G Arnold *et al*, *Phys. Rev. C* **25**, 936 (1982)
[35] G Pastorate, *Nucl. Phys. A* **95**, 694 (1967)
[36] https://shodhganga.inflibnet.ac.in/handle/10603/259972

[37] Y Wang *et al*, *Phys. Lett. B* **802**, 135249 (2020)
[38] B A Li, A T Sustich and B Zhang, *Phys. Rev. C* **64**, 054604 (2001)
[39] P Danielewicz, *Nucl. Phys. A* **685**, 368 (2001)
[40] J Xu, L W Chen, B A Li and H R Ma, *Astrophys. J.* **697**, 1549 (2009)
[41] A Fevre, Y Leifels, W Reisdorf, J Aichelin and C Hartnack, *Nucl. Phys. A* **945**, 112 (2016)
[42] A Fevre, Y Leifels, C Hartnack and J Aichelin, *Phys. Rev. C* **98(3)**, 034901 (2018)
[43] L W Chen *et al*, *Phys. Rev. C* **68(1)**, 014605 (2003)
[44] R S Bhalerao and J Y Ollitrault, *Phys. Lett. B* **641**, 260 (2006)
[45] C Shen and S Alzhrani, *Phys. Rev. C* **102(1)**, 014909 (2020)
[46] B Alver *et al*, *Phys. Rev. C* **77**, 014906 (2008)